Digital Object Identifier 10.1109/IECON.2019.8927087

IECON 2019-45th Annual Conference of the IEEE Industrial Electronics Society

Isolated multiport converter as cost efficient solution for dc-fast charger of electric vehicle

Felix Hoffmann

Jan-Ludwig Lafrenz

Marco Liserre

Nimrod Vazquez

Suggested Citation

F. Hoffmann, J. -L. Lafrenz, M. Liserre and N. Vazquez, "Isolated Multiport Converter as Cost Efficient Solution for DC-Fast Charger of Electric Vehicle," IECON 2019 - 45th Annual Conference of the IEEE Industrial Electronics Society, Lisbon, Portugal, 2019.

Isolated Multiport Converter as Cost Efficient Solution for DC-Fast Charger of Electric Vehicle

Felix Hoffmann, *Student Member, IEEE*,
Jan-Ludwig Lafrenz, *Student Member, IEEE*,
Marco Liserre, *Fellow, IEEE*
Chair of Power Electronics
Christian-Albrechts-Universität zu Kiel
{fho,jll,ml}@tf.uni-kiel.de

Nimrod Vazquez, *Senior Member, IEEE*
Electrical and Electronics Departement
Tecnologico Nacional de Mexico /Instituto
Tecnologico de Celaya
Celaya, Mexico
n.vazquez@ieee.org

***Abstract*—The ongoing electrification of the transport sector raises demands for new power electronic solutions. As a consequence, modular converter structures are state of the art for fast charging, since high power and short charging times are required. This work presents a modular multiport DC-DC converter which has the capability to decrease the cost and size of the required charging station. Furthermore, design guidelines for the investigated topology are presented. The analysis is validated with a three port isolated DC-DC converter with separated loads.**

I. Introduction

Customers value the everyday applicability of electric vehicles (EVs) by the ease of the charging process. Therefore, the availability of chargers and charging duration are of paramount importance. In order to reduce the charging duration, level 3 DC fast charging stations (FCS) have been developed. In early years, the power electronic was placed decentralized in the charging tanks. However, with increasing charging power, the architecture changed to a centralized solution, where the power electronics is located outside the charging tank at a centralized unit. In general, the basic structure of a FCS is shown in Fig. 1(a) and consists of a 50 Hz transformer which steps down the medium voltage (MV) to low voltage (LV). A central rectifier converts the LV-AC to LV-DC, followed by a modular DC-DC stage, in which several isolated DC-DC converters are placed in parallel.

The DC-DC stage is a key component in FCS since it is responsible for voltage isolation and voltage adaption. For the challenging requirements, especially the soft switched converters (LLC, Dual Active Bridge (DAB), Phase Shifted Full Bridge (PSFB)) are well suited as a building block [2]. Apart from the conventional solutions for the isolated DC-DC converter with one input- and one output port (1x1), recently multiport converter architectures have been gaining attention [3]. Especially in micro-grid application with the target to integrated different distributed energy systems [4] [5] [6].

In this work the potential of multiport architectures is evaluated for the application field of FCS: Instead of having several 1x1 isolated DC-DC converter, each unit consist of a 1x2 isolated converter (Fig. 1(b)). Two output ports are magnetically coupled with the input bridge by a multi-winding transformer. This configuration reduces the number of necessary cells and leads to size and cost advantages, which is of particular interest from industry perspective.

However, the combination of the wide output voltage range and the magnetic coupling of the output ports leads to certain design challenges. In particular a Triple Active Bridge (TAB) is investigated. The impact of the coupling strongly depends on the inductance in each of the ports. In previous publications however, the choice of using only the leakage inductance of the transformer [7] or additional external inductance [8] is not further analyzed.

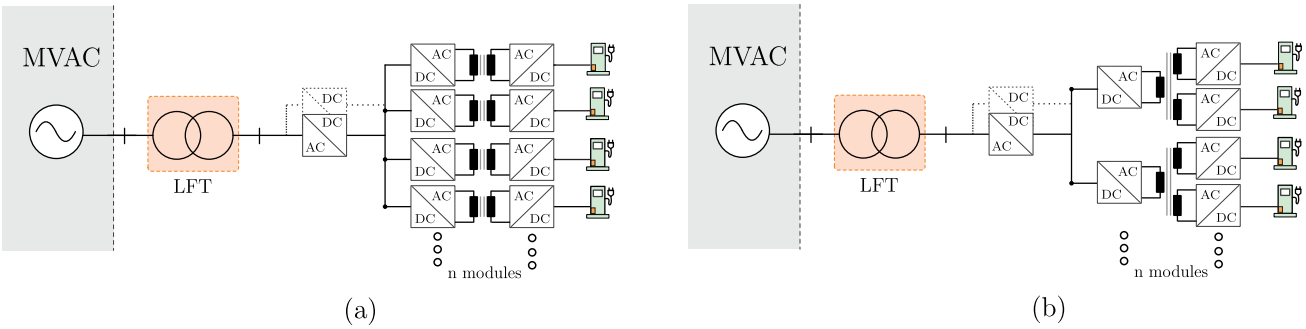

Fig. 1. Fast charging station architectures; (a) Conventional solution with of the DC-DC stage [1], (b) Proposed solution with multiport converter (1x2) as basic building block for the DC-DC stage

Therefore, Section II analyzes the proposed architecture and derives the effects of non-decoupled output charging ports. Section III evaluates the cost saving potential of the proposed architecture. The experimental verification is shown in Section IV, followed by the conclusion in Section V.

II. Proposed Isolated Multiport Converter

The proposed converter is shown in Fig. 2 and consists of three full bridge inverters and a transformer. Each output active bridge considers an inductor in series as part of the converter, in order to diminish the effect of the parasitic elements of the transformer, and avoid the coupling.

All ports are operated to produce a square output voltage, the input bridge voltage is fixed or used as reference, and the other two active bridges are operated independently with the proper phase displacement (δ_1,δ_2) referred to the input bridge in order to regulate its output voltage. The main waveforms of the converter are shown in the Fig. 3.

An amplitude of $nV_{\rm in}$ is considered for the source ($V_{\rm T}$), this is the secondary output of the transformer; since $V_{\rm C1}$ and $V_{\rm C2}$ are the output voltages, then the voltages $V_{\rm T1}$ and $V_{\rm T2}$ have an amplitude of $V_{\rm C1}$ and $V_{\rm C2}$ respectively. The output voltage may be higher or lower than $nV_{\rm in}$, which results in boost or buck mode operation. The proposal is operated in the boost mode, then $nV_{\rm in} < V_{\rm C1}$ and $nV_{\rm in} < V_{\rm C2}$.

A. Operating mode

The operating mode is described in six stages, but just three are addressed since they are similar for the second half of the period (Fig. 3):

1) From $0 < \theta < \delta_1$. During this stage, the output $V_{\rm T}$ is positive ($nV_{\rm in}$), the voltage $V_{\rm T1}$ and $V_{\rm T2}$ are negative ($-V_{\rm C1}$ and $-V_{\rm C2}$). During this time both inductor currents will be increased.

2) From $\delta_1 < \theta < \delta_2$. The output of $V_{\rm T}$ is still positive and $V_{\rm T2}$ still negative, but the voltage $V_{\rm T1}$ is now positive ($V_{\rm C1}$). During this time the inductor current of one bridge will be decreased and the other increased.

3) From $\delta_2 < \theta < \pi$. The output of $V_{\rm T}$ remains positive, but now the voltages in $V_{\rm T1}$ and $V_{\rm T2}$ are both positive ($V_{\rm C1}$ and $V_{\rm C2}$). The current on both inductor is now decreased until the negative semi-cycle starts.

The angles δ_1 and δ_2 are used to regulate independently each output, then the waveforms can be different depending on the value of each angle. To assure the proper independency of each output the inductors placed in series of each output bridge must be much higher than the parasitic element of the transformer (leakage inductance), this is illustrated in next section.

B. Steady state analysis

The equivalent circuit of the isolated converter, with parameters referred to the primary, is shown in Fig. 4. As it can be observed, the three voltage sources are considered, but also the

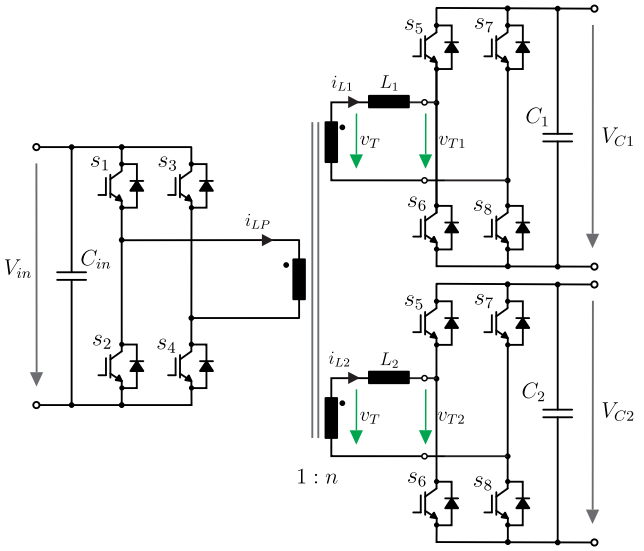

Fig. 2. Investigated topology; Triple active bridge (TAB) with separated outputs forming the charging ports of an EV-charger

inductance of each bridge including the leakage inductance of the transformer. Then $X_{\rm S1} = j\omega(L_{\rm lk,1} + L_{\rm ext,1})$ includes not only the extra inductor, but also the leakage inductance; same happens to $X_{\rm S2} = j\omega(L_{\rm lk,2} + L_{\rm ext,2})$; and for $X_{\rm P} = j\omega L_{\rm lk,P}$ only the leakage inductance of the primary side transformer winding is considered.

The voltage of the middle point considering that $X_{\rm S1} = X_{\rm S2} = X_{\rm S}$ is obtained as:

$$v_{\rm m} = \frac{X_{\rm S}/2}{X_{\rm S}/2 + X_{\rm P}} v_{\rm in} + \frac{X_{\rm S}||X_{\rm P}}{X_{\rm S}||X_{\rm P} + X_{\rm S}} v_{\rm T1} + \frac{X_{\rm S}||X_{\rm P}}{X_{\rm S}||X_{\rm P} + X_{\rm S}} v_{\rm T2} \tag{1}$$

where

- $X_{\rm S}$ is the impedance of the output bridge,
- $X_{\rm P}$ is the impedance of the transformer primary,
- $v_{\rm in}$ is the voltage associated to the input bridge,
- $v_{\rm T1}$ is the voltage associated to the first output bridge, and
- $v_{\rm T2}$ is the voltage associated to the second output bridge.

The value of $v_{\rm m}$ depends on the three voltage sources, and this is the voltage that will determine the final behavior of each output. To avoid the coupling between the different outputs, the next inequality is considered:

$$X_{\rm P} \ll X_{\rm S} \tag{2}$$

Then, using (2), the equation (1) becomes:

$$v_{\rm m} \approx v_{\rm in} \tag{3}$$

While more satisfying (2) the coupling effect between the output bridges will be less, then it is an important fact the value of the extra inductor placed in series to permit the independency of the output voltage regulation.
Considering that equation (2) is satisfied, the waveforms of

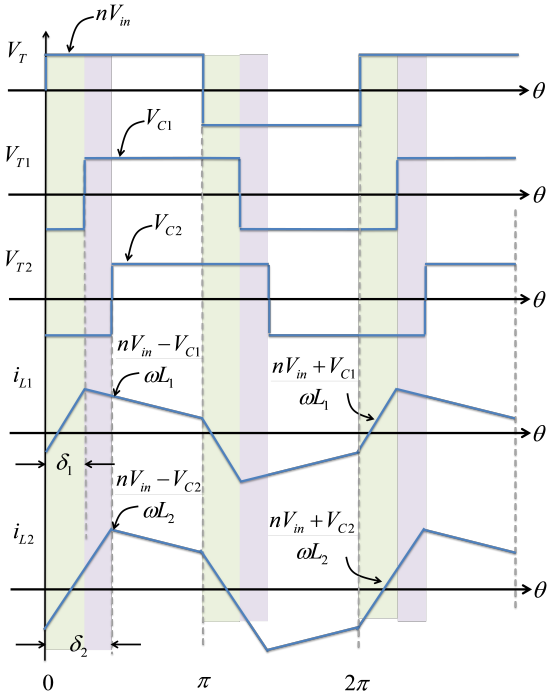

Fig. 3. Main waveforms of investigated TAB topology

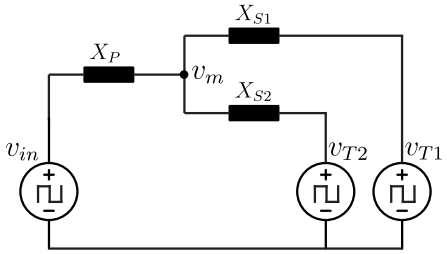

Fig. 4. Equivalent circuit of investigated TAB topology with all parameters referred to the primary side

Fig. 3 are then valid.

The equation of one of the inductor current is described by:

$$i_{\mathrm{L1}}(\theta)=\begin{cases}\dfrac{nV_{\mathrm{in}}+V_{\mathrm{C1}}}{\omega L_1}\theta-I_{\mathrm{i}} & 0\le\theta\le\delta_1\\ \dfrac{nV_{\mathrm{in}}-V_{\mathrm{C1}}}{\omega L_1}\theta+\dfrac{nV_{\mathrm{in}}+V_{\mathrm{C1}}}{\omega L_1}\delta_1-I_{\mathrm{i}} & \delta_1\le\theta\le\pi\end{cases} \tag{4}$$

where: I_{i} is the initial condition of the current.

The before equation is the typical one of the traditional DAB converter, then the following is satisfied at steady state:

$$i_{\mathrm{L1}}(\pi)=\frac{nV_{\mathrm{in}}-V_{\mathrm{C1}}}{\omega L_1}\pi+\frac{nV_{\mathrm{in}}+V_{\mathrm{C1}}}{\omega L_1}\delta_1-I_{\mathrm{i}}=I_{\mathrm{i}} \tag{5}$$

Then the value the initial condition is equal to:

$$I_{\mathrm{i}}=\frac{nV_{\mathrm{in}}-V_{\mathrm{C1}}}{2\omega L_1}\pi+\frac{nV_{\mathrm{in}}+V_{\mathrm{C1}}}{2\omega L_1}\delta_1 \tag{6}$$

The output power is determined by:

$$P=\frac{1}{\pi}\left[\int_0^{\pi}(nV_{\mathrm{in}}i_{\mathrm{L1}})\,\mathrm{d}\theta\right] \tag{7}$$

Then solving, results:

$$P_1=\frac{nV_{\mathrm{in}}V_{\mathrm{C1}}}{\omega L_1}\delta_1\left(1-\frac{\delta_1}{\pi}\right) \tag{8}$$

To obtain the equation for the second output is then

$$P_2=\frac{nV_{\mathrm{in}}V_{\mathrm{C2}}}{\omega L_2}\delta_2\left(1-\frac{\delta_2}{\pi}\right) \tag{9}$$

It is important to remember that equation (8) and (9) are valid if (2) is satisfied.

C. Effect of non-decoupled system

The previous analysis showed that decoupling allows the adjustment of one bridges voltage without any effect on the secondary output voltage, when (2) is satisfied. In this section the effects of a non-decoupled system are analyzed. Therefore, three different design cases are investigated (Fig. 5), which differ in the inductance ratio $l_r=\frac{l_s}{l_p}$ between the secondary and primary side:

- Only external inductance on the primary side bridge and only leakage inductance on the secondary side bridges ($L_p \gg L_s$)
- All bridges have the same inductance ($L_p = L_s$)
- External inductance on the secondary side bridges and only leakage inductance on the primary side bridges ($L_p \ll L_s$)

For the different designs, the phase shift of bridge 1 is increased from $V_{C1}=300V$ to reach a charging voltage of 400 V at port 1. The output voltage of the other bridge (port 2) is kept constant at $V_{C2}=300V$. The specifications for this analysis are given in table I. Due to the coupling through the multi-winding transformer the increase of φ_1 leads to a smaller output voltage at port 2. Hence also the phase shift φ_2 needs to be increased to maintain the required voltage of $V_{C2}=300V$.

TABLE I
SIMULATION SPECIFICATIONS

Input voltage	V_{in} = 300 V
Output voltage 1	$V_{C1}=[300,310,....400]$ V
Output voltage 2	V_{C2} = 300 V
Charger Power	P_{unit} = 50 kW
Switching frequency	f_s = 20 kHz
Nominal PS angle	$\varphi_{nom}=30°$
Transformer turns ratio	$n=1$
Inductance ratio Scenario 1	l_r = 0.5
Inductance ratio Scenario 2	l_r = 1
Inductance ratio Scenario 3	l_r = 10

Fig. 6 shows the effect for the different design scenarios. It can be seen that by increasing the ratio of secondary side to primary side inductance l_r the effect can be minimized.

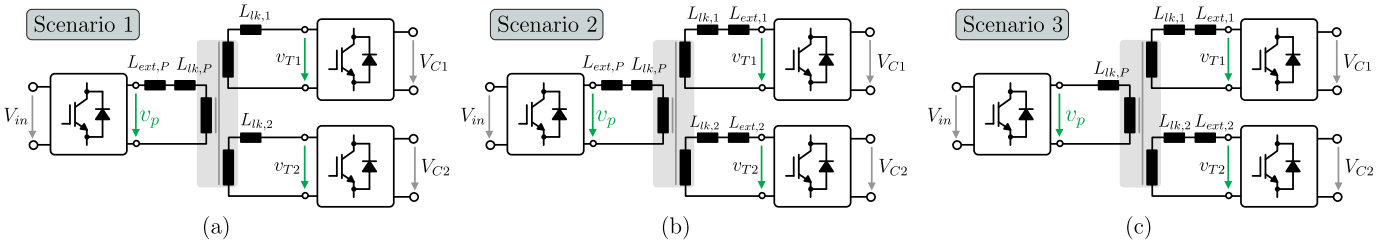

Fig. 5. Different configurations of realizing TAB; (a) Scenario 1: Only external inductance on primary side, (b) Scenario 2: Same inductance in all bridges, (c) Scenario 3: Only external inductances on secondary side

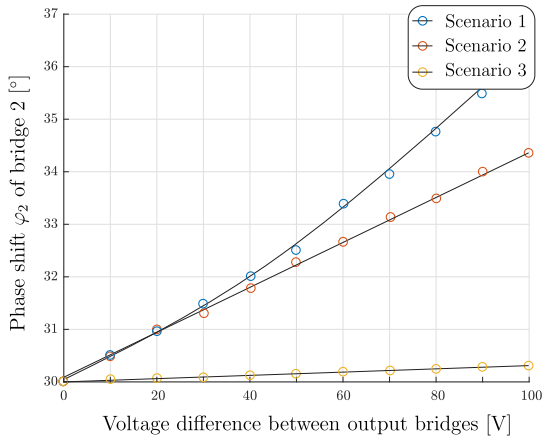

Fig. 6. Effect of different inductance configuration in TAB. The phase shift of output bridge 1 is increased and the necessary phase shift of bridge 2 is shown in order to keep $V_{nom} = 300V$ at port 2

Choosing one external inductor at the primary side (scenario 1) is not recommended, since changes in the output voltage of bridge 1 affect strongly the output voltage of bridge 2. This does not only influence the control effort. But also the required increased phase shift φ_2, to compensate the voltage drop, leads to higher reactive power flow. The relation between higher phase shift and current stresses for the devices has beeen shown in [9].

Additionally, if the primary side inductor is large and the inductance ratio l_r falls below a certain level, the independent controllability of the output voltages might be lost. Changes in one bridge from the primary side to the secondary side will influence the power transfer of the other bridge significantly and cannot be counteracted by changing the phase shift of the affected bridge, due to the very low inductance path between the bridges on the secondary side.

III. Cost Saving Advantages

The reduced number of required hardware leads to cost savings in the design of the FCS. Comparing both approaches, conventional single-winding (SW) architecture (Fig. 7(a)) and multi-winding (MW) architecture (Fig. 7(b)), the number of switching devices can be reduced by 4. Although the remaining 4 switches on the primary side need a higher current rating (considering the same power transfer capability to the charger). Additionally the number of transformer cores can be reduced. In the following the resulting cost advantages are evaluated.

A. Magnetic considerations

The required number of turns is dependent on the magnetic core area A_{ce} and can be calculated with [10]:

$$N_{pri} = \frac{V_{pri}}{k_f f_s A_{ce} B_{pk}} \tag{10}$$

The necessary area for the primary side winding follows as:

$$A_{pri} = N_{pri} A_{con,pri} \tag{11}$$

With the conductor area $A_{con,pri}$ which can be calculated with the maximum primary RMS current through the winding and a defined maximum current density $J = 4\frac{A}{mm^2}$ of the wire. The same principle can be applied for the secondary side winding. As a result, the sum of the required area for the windings needs to fit in the available core window area.

Since the input voltage of both cases shown in Fig. 7(a),(b) is the same, it follows with (10) that the required magnetic core area A_{ce} remains constant for the same number of turns. However in the case of MW approach, the primary winding needs an increased conductor size, since two charging ports are served by only one primary winding. Hence, the required window area for the primary winding in the MW approach is twice compared to a primary winding in the SW approach. The reduction of one primary winding is compensated by

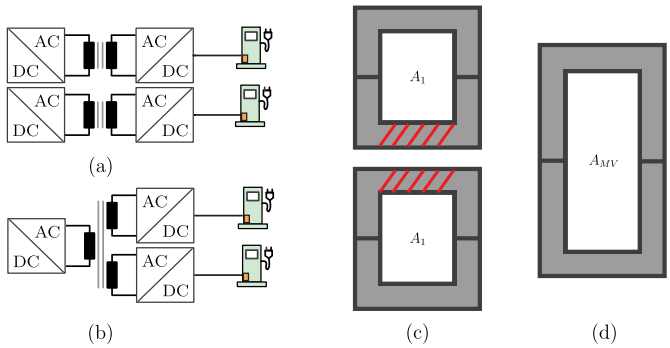

Fig. 7. Different magnetic configurations, (a) Single-winding (SW) architecture (1x1), (b) Multi-winding (MW) architecture (1x2), (c) U-core for SW architecture with volume reduction potential (marked red), (d) U-core for MW architecture (1x2)

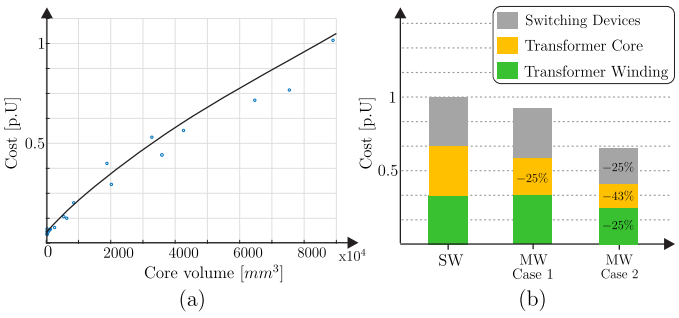

Fig. 8. Cost relationship, (a) Costs in dependency of magnetic core volume for different N-87 Ferrit U-cores,(b) Transformer and device cost saving potentials for MW architecture

the larger conductor size. In total the required window area remains constant ($2A_1 = A_{MV}$).

From Fig. 7(c),(d) it becomes obvious, that a volume reduction of the magnetic core is possible since the mean length l_{AV} can be reduced by approximately a factor of $\frac{1}{4}$ in the MW approach (assuming quadratic core structure). Hence for the required volume for both approaches follows:

$$V_{SW} = A_{ce} l_{AV} \tag{12}$$

$$V_{MW} = A_{ce} \frac{3}{4} l_{AV} \tag{13}$$

In order to quantify this effect, different N87 U-cores are collected and prices are compared with respect to magnetic core volume and price (Fig. 8(a)). The linear characteristic of the core volume and the magnetic costs leads to the conclusion that the MW approach can reduce core cost by a factor of $\frac{1}{4}$.

B. Switching device considerations

A similar analysis is performed for the switch related costs. Therefore, the relationship between costs and different current rated SiC devices from manufacturer *Wolfspeed* are evaluated. Approximately a linear behavior between the $r_{DS,on}$ and the costs can be assumed from 40 mΩ on to higher values.

C. Overall cost savings

The overall cost saving potentials are shown in Fig. 8(b). The first MW case 1 assumes that the primary bridge in Fig. 7(b) has the same power transfer capability like the sum of the primary units in the SW approach in Fig. 7(a). Hence two cars can charge with the maximum rated power. The magnetic core cost reduces by 25 %. The switch costs remain approximately constant due to the linear behavior between costs and $r_{DS,on}$. Similar the copper winding costs remain constant, since the reduction of one primary winding is compensated by the required increased primary conductor size.

The MW architecture brings more flexibility with respect to the power transfer capability. A second design approach (MW case 2) is analyzed in which the power rating of the MW primary side bridge in Fig. 7(b) is the same to one SW primary bridge in Fig. 7(a). This means that each charger can provide maximum rated power, only when one charger is used. Especially for scenarios where in the majority of times not all chargers are used simultaneously, this design is beneficial. Similar concepts, which reduces the power transfer capability when more chargers are used in a charging park are common practice. In this scenario the cost advantages becomes even more severe (Fig. 8(b)).

It should be mentioned, that only switches and transformer cost improvements are considered. However, it should be pointed out, that especially the saved costs for PCB, gate driver and other auxiliary power equipment can have a huge saving potential. These costs are very design specific and cannot be generalized. Therefore, they are not considered in detail.

IV. Experimental Verification

A TAB prototype with a MW transformer was constructed (Fig. 9(a)). As a reference point of the analysis, the voltages at the charging ports are assumed equal ($V_{T1} = V_{T2} = 250V$) and hence δ_1=δ_2.

Similar to the simulation analysis, in one output bridge (port 1), the relative phase shift δ_1 is changed in order to increase the charging voltage V_{T1} from 250V to 350V. As a difference to the simulation, the relative phase shift δ_2 of the other bridge (port 2) is kept constant. The resulting output voltage changes at port 2, due to the coupling, are analyzed. Specifications for the experimental setup are given in table II.

In order to prove the concept of decoupling, the ratio l_r of the secondary and primary side inductance is varied and the effect of the coupling, in terms of voltage variation at port 2, is observed. Results are shown in Fig. 9(b)-(d). Whereas the blue curve represents the AC input voltage v_p, the green curve the AC voltage of port 1 v_{T1}, the light blue curve the AC voltage of port 2 v_{T2} and the pink curve the primary side transformer current. The value of l_r is rising from Fig. 9(b)-(d).

For the lowest l_r ratio the voltage of port 2 v_{T2} drops from 250V to 208V (Fig. 9(b)) if the phase shift δ_2 of port 2 remains unchanged. This shows the strong coupling for this case. To compensate the voltage drop of port 2 the phase shift of port 2 needs to be increased. It can be further seen that by increasing the l_r ratio, the voltage drop of v_{T2} at port 2 becomes smaller. For the case of highest l_r ratio, the voltage of port 2 v_{T2} is almost constant at 250 V (Fig. 9(d)).

TABLE II
Experimental Setup Specifications

Input voltage	$V_{in} = 300$ V
Output voltage 1	$V_{C1} = [250, 260, ...350]$ V
Output voltage 2	$V_{C2} = 250$ V
Switching frequency	$f_s = 20$ kHz
Transformer turns ratio	$n = 1$
Inductance ratio Scenario 1	l_r = 1
Inductance ratio Scenario 2	l_r = 5
Inductance ratio Scenario 3	l_r = 10

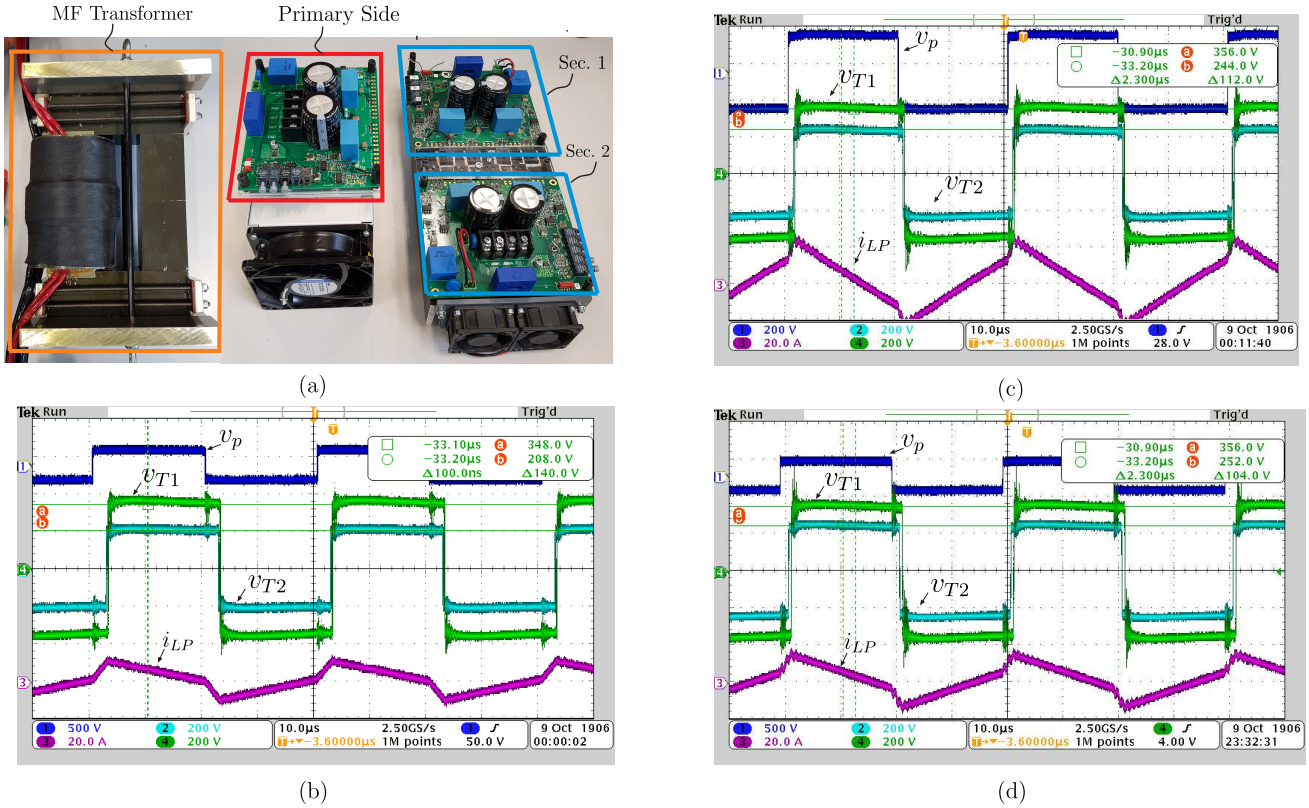

Fig. 9. Effects of power transfer coupling to unchanged port 2 with the target to keep output voltage constant at 250V in dependency for different inductance ratios l_r, (a) TAB Set-up, (b) Test with inductance ration $l_r = 1$, (c) Test with inductance ration $l_r = 5$, (d) Test with inductance ratio $l_r = 10$

V. Conclusion

This paper analyzed the potentials and challenges of using a multiport converter, in particular TAB converter, in FCS. Based on the specific requirements in the application field of FCS, the effect of different transformer inductances is evaluated. To reach best decoupling between two charging ports, the secondary side inductance should be higher compared to primary side inductance. External inductances should only placed on the secondary side. As shown in the analysis, the best decoupling leads to less necessary phase shift adaption and hence to a better performance of the converter. Furthermore the cost advantages of the TAB converter in FCS has been demonstrated and the operation validated experimentally.

VI. Acknowledgment

'This work was supported in part by the European Union/Interreg V-A - Germany-Denmark, under the PE:Region Project and in part by the European Research Council under the European Unions Seventh Framework Programme (FP/2007-2013)/ERC Grant 616344-HEART and by the mexican side the work is sponsored by CONACyT under project No. 291626 (I0000/727/2017).

References

[1] Enercon e-charger 600 leaflet. [Online]. Available: https://www.enercon.de/fileadmin/Redakteur/Service/EC_E-Charger_600_en_web.pdf

[2] M. Yilmaz and P. T. Krein, "Review of battery charger topologies, charging power levels, and infrastructure for plug-in electric and hybrid vehicles," *IEEE Transactions on Power Electronics*, vol. 28, no. 5, pp. 2151–2169, May 2013.

[3] S. Falcones, R. Ayyanar, and X. Mao, "A dcdc multiport-converter-based solid-state transformer integrating distributed generation and storage," *IEEE Transactions on Power Electronics*, vol. 28, no. 5, pp. 2192–2203, May 2013.

[4] Savitha K.P and P. Kanakasabapathy, "Multi-port dc-dc converter for dc microgrid applications," in *2016 IEEE 6th International Conference on Power Systems (ICPS)*, March 2016, pp. 1–6.

[5] Junjun Zhang, Hongfei Wu, Jun Huang, Yan Xing, and Xudong Ma, "A novel multi-port bidirectional converter for interfacing distributed dc micro-grid," in *2014 IEEE 23rd International Symposium on Industrial Electronics (ISIE)*, June 2014, pp. 2344–2348.

[6] K. Venugopal and P. Kanakasabapathy, "Three port multi winding flyback converter for dc microgrid applications," in *2017 International Conference on Technological Advancements in Power and Energy (TAP Energy)*, Dec 2017, pp. 1–6.

[7] R. Chattopadhyay, G. Gohil, S. Acharya, V. Nair, and S. Bhattacharya, "Efficiency improvement of three port high frequency transformer isolated triple active bridge converter," in *2018 IEEE Applied Power Electronics Conference and Exposition (APEC)*, March 2018, pp. 1807–1814.

[8] Yue Yu, K. Masumoto, K. Wada, and Y. Kado, "Power flow control of a triple active bridge dc-dc converter using gan power devices for a low-voltage dc power distribution system," in *2017 IEEE 3rd International Future Energy Electronics Conference and ECCE Asia (IFEEC 2017 - ECCE Asia)*, June 2017, pp. 772–777.

[9] L. F. Costa, F. Hoffmann, G. Buticchi, and M. Liserre, "Comparative analysis of multiple active bridge converters configurations in modular smart transformer," *IEEE Transactions on Industrial Electronics*, pp. 1–1, 2018.

[10] M. K. Kazimierczuk, *High-Frequency Magnetic Components*. Wiley, 2014.